
MULTISENSOR SYSTEMS AND FLOOD RISK MANAGEMENT. APPLICATION TO THE DANUBE DELTA USING RADAR AND HYPERSENSPECTRAL IMAGERY

Simona NICULESCU⁽¹⁾, Cédric LARDEUX⁽²⁾, Fábio GÜTTLER⁽¹⁾, Jean-Paul RUDANT⁽²⁾

⁽¹⁾ Géomer, UMR 6554, LETG, Technopôle Brest Iroise, Place Nicolas Copernic, 29280, France
e-mail : simona.niculescu@univ-brest.fr ; fabio.guttler@univ-brest.fr

⁽²⁾ UMLV, Institut Francilien des Géosciences, 5 bd Descartes, 77454 Marne la Vallée Cedex 2, France
e-mail: lardeux@univ-mlv.fr

Soumis le 23 mars 2009; accepté le 6 décembre 2010 - © Revue Télédétection, 2010, vol. 9, n° 3-4, p. 271-288

RESUME

En ce début de 21^e siècle, le risque d'inondation constitue encore le risque majeur au monde (avec les tempêtes, les inondations représentent 60% des catastrophes naturelles) et le réchauffement climatique pourrait encore renforcer ce phénomène à l'avenir. En Europe, malgré toutes les politiques et les mesures prises, au cours des dernières décennies, de grandes inondations ont lieu quasiment chaque année. Les actualités confirment régulièrement la réalité et la prégnance du risque d'inondation en Europe. Cet article présente une application concernant le risque d'inondation durant les événements du printemps 2006 dans le delta du Danube en exploitant des images radar ENVISAT/ASAR et l'imagerie hyperspectrale CHRIS/PROBA en matière d'analyse et de cartographie des zones inondées et de la classe de l'inondable. L'utilisation couplée des techniques spatiales (radar et hyperspectrale) pourrait contribuer à une meilleure compréhension des phénomènes liés aux inondations dans le Delta du Danube, ainsi qu'à la gestion de ce risque dans le delta et à son développement durable. Dans la partie Gestion du risque, ce travail aborde des aspects méthodologiques liés à la caractérisation de l'aléa de l'inondation tandis que dans la partie Prévision, la connaissance et la modélisation de l'Occupation du sol seront abordés. Des méthodes des noyaux (kernels), adaptées en particulier à la mise en évidence des variations spatio-temporelles - Support Vector Machine – ainsi que des méthodes basées sur le principe de la logique floue (classifications orientées objet) sont mis en place afin d'obtenir le plan d'information des données spatiales.

Mots clés : delta du Danube, risque d'inondation, images radar Envisat/Asar, aléa de l'inondation, images hyperspectrales Proba/Chris, occupation du sol de l'inondable.

ABSTRACT

At the beginning of the 21st century, flood risk still represents a major world threat (60% of natural disasters are initiated by storms) and the climate warming might even accentuate this phenomenon in the future. In Europe, despite all the policies in place and the measures taken during the past decades, large floods have occurred almost every year. The news regularly confirms this reality and the serious threat posed by flood risks in Europe. This paper presents an application to the Danube Delta exploiting radar imagery ENVISAT/ASAR and hyperspectral imagery CHRIS/PROBA for mapping flooded and floodable areas during the events of spring 2006. The uses of multisensor systems, such as radar and hyperspectral imagers, contribute to a better comprehension of floods in this wetland, their impacts, and risk management and sustainable development in the delta. In the section Risk management, this paper approaches the methodological aspects related to the characterization of the flood hazard whereas in the section Forecasting we will focus on the knowledge and modeling of the Land cover. The method of kernels, particularly adapted to the highlighting of the special-temporal variations - Support Vector Machine – and the methods based on the principle of the vague logic (object-oriented classifications) will be implemented so as to obtain the information plan of the spatial data.

Key words: Danube Delta, flood risk, ENVISAT/ASAR radar images, flood hazard potential, Proba/Chris hyperspectral images, land cover of floodable.

1. INTRODUCTION

1.1. Context

At the beginning of the 21st century, the flood risk still represents a major world threat (60% of the natural catastrophes) and the climate warming might even accentuate this phenomenon in the future. In Europe, despite all policies and taken measures, during the past decades, great floods took place almost every year. The news regularly confirms the reality and serious threat posed by the flood risk in Europe. A rapid analysis of the flood situation after 1998 shows us troubling statistics – more than 100 serious floods until 2002, out of which catastrophic ones along the Danube and Elba in 2002 partially repeated in 2006. In 2005 and 2009, other areas of the Central and Eastern Europe were affected by disastrous floods. The list might continue with the events of 2010, Xynthia storm that rushed into the French west, the floods from last June-July that violently hit several European regions. At the hands of such a recurrent situation, several European measures were taken, the European system against floods (*European Flood Alert System*), flood risk prevention plans (*PPRI*) in France, and the European Committee has adopted the directive 2007/60/EC related to the evaluation and management of the flood risks¹ at the level of the large European basins. The new scientific means, the computation methods, the numerical models for land and satellite images facilitated and made possible their study at these levels, making the difference between the rise in water level and the phenomenon level. A very precious help that could improve the efficiency of these analyses might be systematically given by the actions of the Plan *Space and major catastrophes*.

1.2. State of the art

By dealing with two major aspects of flood risk, namely *Integrated Risk Management* (methodological aspects related to characterization of the *flood hazard potential*) and *Forecasting* (the knowledge and modeling of *Land use*), this paper will also take into consideration the topical elements (vulnerability and local context) of the analyzed territory.

Current studies in *hazard potential determination* focus on the development of a statistical/stochastic approach, proposing determining and probabilistic models. According to certain researchers (Vidal, 2005), in order to be reliable, hydraulic models must be restricted, via a closing system, due to flood related knowledge (water levels, volume transiting the plain the moment the flood passes, etc.). According to several authors (Aronica and *al.*, 1998; Pappenberger and *al.*, 2005), these data are, most of the times, difficult to obtain on field. One solution could be the exploitation of the water levels estimated based on radar satellite images during floods. The methods relying on the measurement of the radar retro-diffusion coefficient based on high resolution data have been the object of L-band (Ulaby and *al.*, 1983) and C –band (Fella and *al.*, 1997; Brown and *al.*, 1997) development; the water levels were estimated with the help of the limits of flood prone areas, extracted from C band radar satellite images, and topographic maps (Brakenridge and *al.*, 1998). The obtained uncertainties (between 1 and 3 meters) were considered incompatible with the accuracy necessary for hydraulic modeling. To improve the delineation of the shoreline in areas of flooded vegetation, Horrit and *al.* (2000) use vegetation heights derived from lidar data. In a similar approach to that developed by Puech and Raclot (2002) for aerial photography, Hostache et *al.* (2005 and 2009) apply a dept-mapping method to a SAR flood image using high-precision photogrammetric data (uncertainty of 30 cm on average).

The crisis management phase involves the production of mapping documents which localize the event and its extent. There are several methods for obtaining an information plan concerning space data, such as photo-interpretation, image segmentation, that make use of mathematic principles, such as contour detection, fuzzy logic with data mining or artificial neural networks. Many SAR image-processing techniques exist to more or less successfully derive flood area or extent, including simple visual interpretation (Oberstadler and *al.*, 1997), image histogram thresholding (Brivio and *al.*, 2002; Matgen and *al.*, 2004, 2007), automatic classification algorithms (Bonn and Dixon, 2005), image texture algorithms (Schumann and *al.*, 2005, 2009), and multitemporal change detection methods (Laugier and *al.*, 1997). Numerous studies (Marinelli and *al.*, 1997; Nico and *al.*, 2000; Yésou and *al.*, 2000; Alsdorf and *al.*, 2007) emphasized the important contribution of phase coherence variation, obtained starting from an interferometric pair of radar images, which completes the study of signal amplitude.

If access to the hydric basin side has major advantages as concerns the modeling stage, knowledge of *land use* is at least as important. Land use management (with the objective of establishing a connection between land settlement and risk management) is considered, together with crisis forecasting and management, the most useful instrument for flood prevention (Grundfest and Handmer, 2001).

The measures for land use management in flood-prone areas are hindered by numerous conflicts related to territorial practices. The Americans approach floods from a different angle – via the optimization of the management of a flood-prone area, depending on the socio-economic and environment profitability objectives (Pasterick, 2000).

¹ This directive demands the Member states a preliminary evaluation in 2011 so as to identify the high-risk river basins and the coastal areas. In 2013, they will also have to make up a map of the floodable areas and to implement in 2015 risk management plans focused on the prevention, protection and reaction capacity.

Many different image processing techniques exist to derive flood area or extent from SAR (for a variety of techniques). However, classification accuracies of flooded areas and especially of floodable areas (most of the time defined as a ratio of the total area of interest where classification errors are omitted) vary considerably and only in rare cases do they reach 90% (Schumann, 2009). Interpretation errors may arise from a variety of sources: inappropriate image processing algorithms, altered backscatter characteristics, unsuitable wavelength and/or polarizations, unsuccessful multiplicative noise (speckle) filtering, remaining geometric distortions, and inaccurate image geocoding.

Traditional multispectral images and outdated remote sensing processing techniques are currently insufficient for well-suited researches in complex landscapes, such as deltaic zones. In this context, the testing of new advanced data and non traditional analysis approaches becomes a challenge.

Hyperspectral remote sensing is a relatively new technology, which is currently being investigated by researchers and scientists with regard to the detection and identification of minerals, ground vegetation and man-made materials (Jung *et al.*, 2004). According to Bannari *et al.* (2006), the significance of hyperspectral remote sensing lies in its capability to acquire a full reflectance spectrum for each pixel in the imagery. The reflectance spectrum in the 400–2500 nm regions can be utilized to distinguish a large variety of surface cover materials, which is not possible with broadband sensor technology.

2. STUDY AREA AND DATASET

2.1. Danube Delta

The drainage basin of the Danube, situated in the interior of Central Europe, occupies about 10% of the entire area of the European continent and it is relatively symmetric: 44% of its total area stretches on the right bank, 56% on the left bank (figure 1). The Danube Delta with an area of 3510 km², without the Razim Sinoe lagoon complex, has the shape of a triangle whose tip is oriented westwards whereas its basis is situated eastwards, all along the Black Sea coast (figure 2). Among the three main branches, the Chilia in the north, the Sulina in the central part and the St. George in the south, the delta is made up of a multitude of channels, canals, floating islands and lakes (8.9% of the delta). The last two main branches have been rectified several times and 93.3% of the delta area is between –1 m and +2 m from the Black Sea mean level and 79.5% is under the 0 m level, meaning that almost two thirds of the total areas of the delta are permanently submerged.

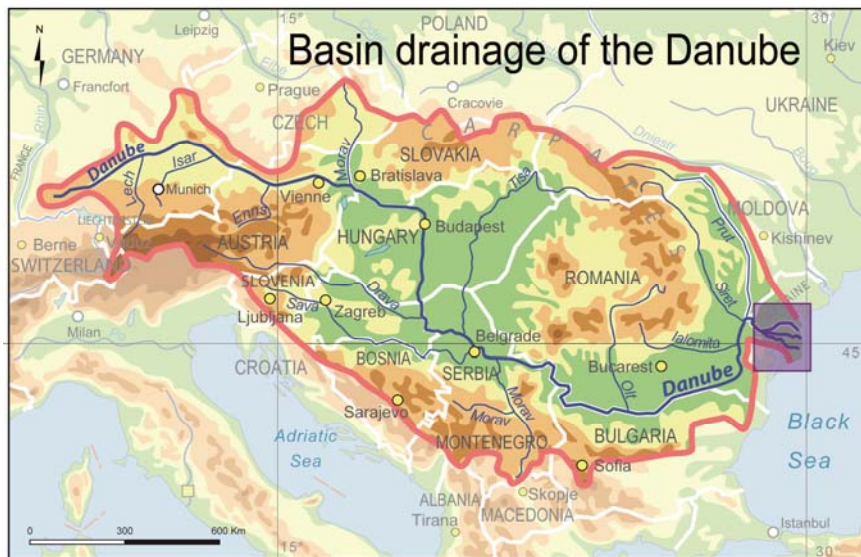


Figure 1. Basin drainage of the Danube

The analysis of the hydrological functioning of the delta shows that the delta floodability is conditioned by its hypsometric particularities (the maximum altitude is 14 m and the minimum one reaches – 2.5m in the riparian depressions), as well as by the amplitude and the periodicity of the maximum levels of the Danube. We should also add the effect of the delta management, especially the building of dams starting from the 1950's what has considerably reduced the floodable areas of the delta. The current length of the dams is 1030 km, namely 29.3% from the dyked surface of the delta (figure 2). The floods of the Danube delta clearly coincide with the periods when the river level has risen. The multiannual measurements of Tulcea hydrograph (figure 3) indicate three periods of maximal levels of

the river: at the end of January and the beginning of February, in spring in May-June and in autumn at the end of November (figure 3).

Over the centuries, serious risings have been recorded reaching maximum levels in 1895 (13,700 m³/s), 1942 (13,387 m³/s), 1970 (14,520 m³/s), 2006 (15,800 m³/s). Analyses of the recorded flows in different points of the Danube show that they most frequently occur in April and May (figure 3).

From February to April 2006, several European rivers, especially the Danube and the Elba overflowed following heavy rains conjugated with snowfalls. In Romania, 400 localities suffered from the ravaging attacks of the incessant rains. 22 of the 47 counties of the country were affected by the worst floods recorded for 110 years, the south-western and south-eastern regions being especially affected. The Danube often reached 4.9 m and, at the mouth of the delta (at Tulcea, figure 3), the swelling of the Danube reached levels two times higher than the normal level. After the floods from the spring of 2006, the Danube delta was hit by the most important drought since 1947 during the summer of 2007 (figure 3). In our researches, we have shown an image and hydrological data for the summer of 2007 so as to compare and take into consideration two situations out of the ordinary succeeding one another within one year interval.

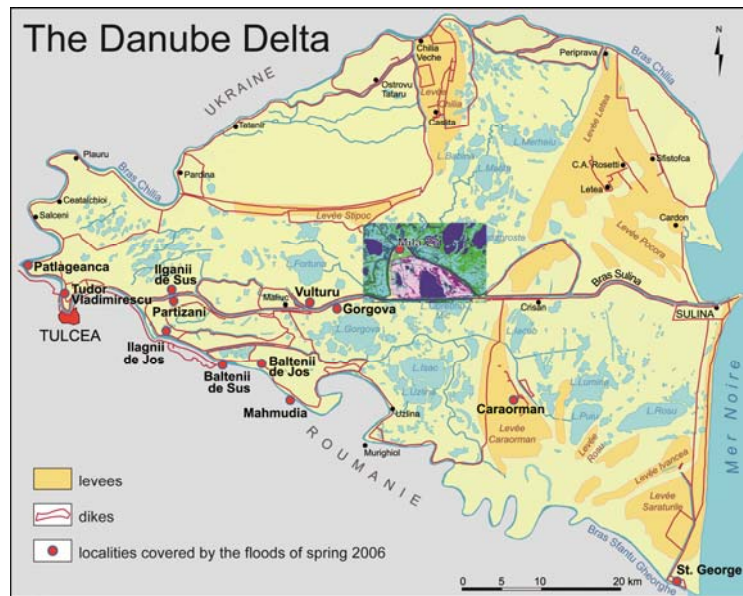


Figure 2. The Danube Delta and Mila 23

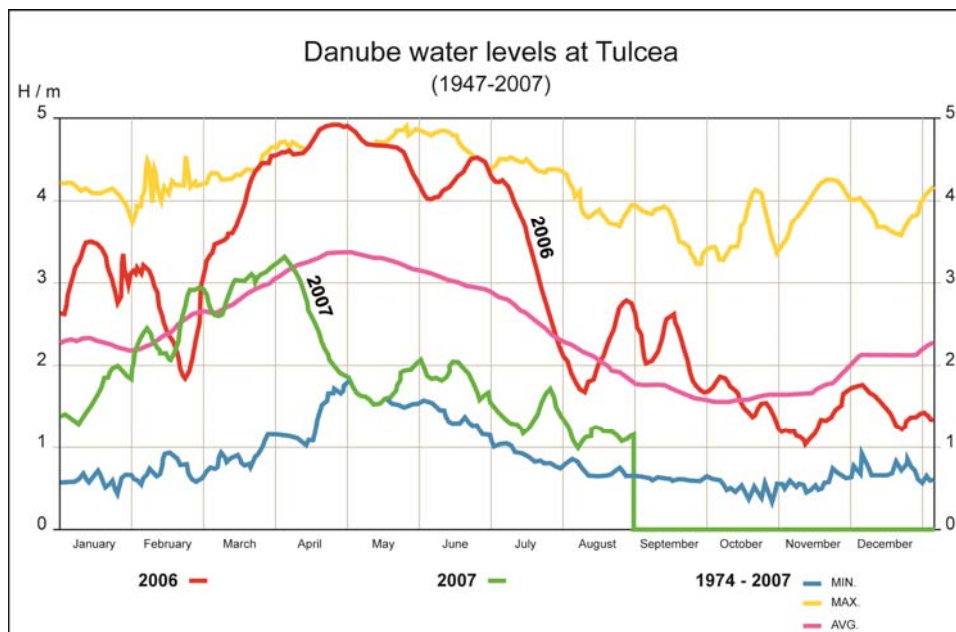


Figure 3. Danube water levels at Tulcea (1947-2007)

2.2. Datasets

2.2.1. Radar dataset

The data are composed of ASAR data (C band, $\lambda=5.6\text{cm}$). The ASAR data are in the Wide Swath Mode with a resolution of 150m and a pixel spacing of 75m. The table 1 shows the different dates of acquisition. The radar sensors operating in C band and placed in orbit since 1991, such as those aboard the ERS or RADARSAT satellites, have already proven their capacities for mapping floods. The ASAR sensor, placed in orbit in 2002, and assuring the continuation of observations performed by satellite-borne radars, offers a useful tool for the monitoring of floods over the survey site.

ASAR radar of ENVISAT gives images with two simultaneous polarizations (HH and HV; HH and VV; or VV and VH) and allows for multiple data capture configurations with a wide range of incidence angles (15° to 45°) and spatial resolutions (30, 150 et 1000 m).

The hydrogram presented here shows the passing of ENVISAT satellite in relation with the flows of the Danube at Tulcea at the entrance in the delta between March 30th 2006 and May 20th 2006 (figure 4).

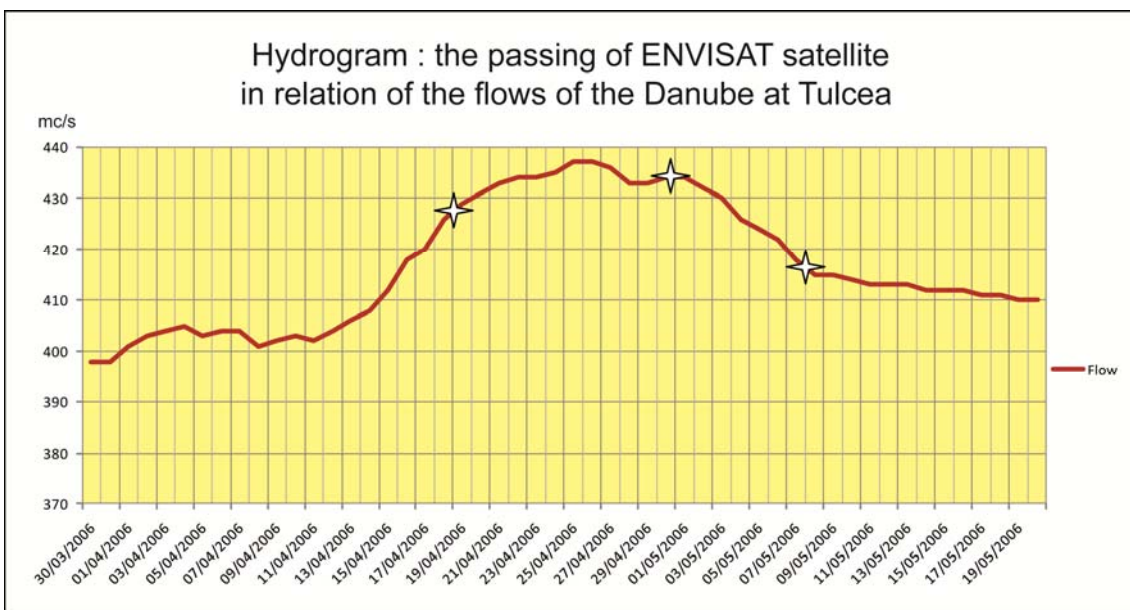


Figure 4. Hydrogram : the passing of ENVISAT satellite in relation of the flows of the Danube at Tulcea

Table 1. Radar dataset

ASAR mode	Date
WSM Ascending	06/13/07
WSM Descending	05/08/06
WSM Ascending	05/01/06
WSM Descending	04/19/06

2.2.2. Hyperspectral dataset

The PROBA (Project for On-Board Autonomy) satellite was launched on October 22, 2001 by the European Space Agency (ESA). This CHRIS instrument is also the first satellite mounted hyperspectral sensor to have a high spatial resolution and programmable spectral bands. This instrument provides a ground sampling distance of 17 m, at perigee, over typical image areas of 13 km². It has a spectral range from 400 to 1050 nm, at a spectral resolution of <11 nm (Cutter, 2004).

One CHRIS/PROBA image (mode 2, water bands), representing the central part of the Danube Delta (around the Mila 23 settlement), was used in this study (figure 2). It was acquired on 17th December 2004 with the following band wavelengths (table 2).

Having as a goal the observation and mapping of the land cover in the floodable delta, the choice of an image from the period of Danube's low levels (December-January, in normal conditions when the Danube's level was 2.30m as compared to 4.26m on April 19th 2006) seems quite pertinent to us.

The multi-angle view capability provided by the PROBA platform has several applications, potentially improving image classification and the quantification of vegetation structure and function.

A synthetic table (table 3) connects the data used, their significance in relation with the main events from the delta in 2006 (floods), 2007 (drought) and the implementation methodology.

Table 2. Dataset / Processing Image / Objectives

Band	Min λ (nm)	Max λ (nm)	Width λ (nm)	Band	Min λ (nm)	Max λ (nm)	Width λ (nm)
W1	406	415	10	W10	646	656	10
W2	438	447	9	W11	666	677	11
W3	486	495	9	W12	677	683	6
W4	505	515	10	W13	683	689	6
W5	526	534	9	W14	700	712	12
W6	556	566	10	W15	752	759	7
W7	566	577	8	W16	773	788	15
W8	585	596	12	W17	863	881	18
W9	618	627	9	W18	1003	1036	33

3. METHODS

3.1. Introduction

From the methodological viewpoint, this article proposes a multisource analysis of the radar and hyperspectral data in terms of *Forecast and Flood Risk Management* in the Danube delta for the events from the 2006 spring. First, they propose an algorithm based on the use of the kernel functions which are used to project the different data in a superior dimension as they are linearly separable for the treatment of the radar data. We speak about the *Support Vector Machine*. SVM belongs to the new learning methods developed on the basis of the Statistical Learning Theory of Vapnik and Chervonenkis (Vapnik, 1995). One of these methods called Support Vector Machine (Cortes et al., 1995), allows for the making of estimations for classification (two classes or more) (Burges, 1998) or for regression (Smola and al., 1998). This method has been chosen since we speak of a method based on active learning allowing for the selection of a pertinent learning assembly, generally smaller, which offers a shorter calculation time and a better generalization (Schohn and Cohn, 2000). This stage of data classification is followed by a fusion of the radar data. The basic principle of this methodological stage is the fusion of multiple data related to the delta floods so as to obtain a more reliable judgment than the one obtained by the group of sources taken each one separately. The dataset of the merged data regards 3 dates from the 2006 spring, a real image before the flood peak, an image during it and an afterwards image with an image from 2007 summer during the most serious draught since 1947 in the delta. The interest of this diachronic approach is, on one hand, to observe and map the flooded areas during the 2006 flood and, on the other hand, to observe, define and map the class of areas liable to flooding. As for the hyperspectral data, the treatment belongs to the object-oriented classifications. In the object-oriented analysis, the basic unit is the object or segment and not the pixel. Thus, it might better answer the remote sensing expectations: extracting objects corresponding to reality in terms of shape and thematic content (M. Baatz et al., 2000, 2004). The essential objective of this methodological approach is to characterize the areas liable to flooding of the delta, to bring clarifications on the soil occupancy regarding the areas liable to flooding for a period (autumn/winter) considered normal from the hydrological and meteorological viewpoint. In case of the hyperspectral data, the analysis solely refers to the geographical area situated almost in the middle of the delta (figure 2).

3.2. Support Vector Machine

The Support Vector Machine relies on the use of the kernel functions (Shawe-Taylor J. and Cristianini N., 2004; Bishop C., 2006; Kanevski M. and *al.*, 2009) that are used to project the different data in a superior dimension as they are linearly separable. They define a hyperplane so as to better separate the learning data.

In linear case let us consider a two class classification problem with P training samples. Each sample is described by a N dimension vector V_j ($j \leq P$), belonging to an input space E (with the same dimension N). The N vector components are also called primitives, or in the present case polarimetric indices. The label of the j^{th} sample V_j is Y_j . For a two class problem, the class labels are -1 or +1 (*i.e.* $Y_j \in \{-1; +1\}$).

The classification problem consists in finding an hyperplane (*i.e.* a subspace of dimension $N-1$), separating the two classes. Such an hyperplane is defined by its normal vector ω and an offset b . The classification function f defining the label Y_j of the sample V_j that is considered here is defined following (equation 1) :

$$f(V_j) = \text{Sign}(\langle \omega, V_j \rangle + b) = Y_j \quad (1)$$

where Sign is the sign function, and $\langle \omega, V_j \rangle$ represents the scalar product between ω and V_j . The vectors subset corresponding to the training samples which are closest to the considered hyperplane is called the Support Vector (figure 5).

The distance between the Support Vector and the considered hyperplane is called the margin and is equal to $\frac{1}{\|\omega\|}$, where $\|\omega\|$ refers the norm of the ω vector. The goal of the SVM is to compute the optimal hyperplane separating the two classes, or equivalently to maximize the margin by finding the min ($\|\omega\|$).

The Lagrangian formalism makes it easier to realise this optimization, by solving the following equation 2 :

$$f(V_j) = \text{Sign}\left(\sum_{i=1}^P Y_i \alpha_i \langle V_j, V_i \rangle + b\right) \quad (2)$$

where α_i are the Lagrange multipliers.

The presence of noise in the data can be accounted for by defining a distance tolerating the data scattering, corresponding to the so-called *slack variable*, thus relaxing the decision constraint. The optimal margin is in this case is called the soft margin.

In non linear case, when no hyperplane can be found in the input space E between the 2 classes (figure 6), the training vectors are projected into a space H of dimension M ($M > N$), named the feature space, where such an hyperplane exists. The projection is realized through the function Φ ($\Phi: \mathcal{R}^N \rightarrow H$). In this case, equation 2 becomes in the space H (equation 3) :

$$f(V_j) = \text{Sign}\left(\sum_{i=1}^P Y_i \alpha_i \langle \Phi(V_j), \Phi(V_i) \rangle + b\right) \quad (3)$$

Actually, it is not necessary to project the data sets in the space H through the function Φ as only the scalar product defined in the feature space H has to be performed. In this case, it is equivalent to a function K , named the kernel function, which verifies (equation 4) :

$$K(V_j, V_i) = \langle \Phi(V_j), \Phi(V_i) \rangle \quad (4)$$

through which Eq. 3 becomes (equation 5) :

$$f(V_j) = \text{Sign}\left(\sum_{i=1}^P Y_i \alpha_i K(V_j, V_i) + b\right) \quad (5)$$

Three kernels are commonly used :

The polynomial kernel

$$K(V, V_i) = (\langle V, V_i \rangle + 1)^p$$

The sigmoid kernel

$$K(V, V_i) = \tanh(\langle V, V_i \rangle + 1)$$

The Radial Basis Function (RBF) kernel

$$K(V, V_i) = \exp -\frac{|V - V_i|^2}{2\sigma^2}$$

There are no general rules for the choice of the kernel function. After several tests, better results are obtained with the same parameterization as Fukuda and Hirosawa, 2001, *i.e.* with a RBF kernel, with $\sigma = 0.5$ and a cost parameter equal to 1000.

The principle of SVM has been developed for a two-class problem but can be easily extended to a multi-class problem by considering for example the “ One Against All ” (OAA) or the “ One Against One “ (OAO) algorithms. If K classes are to be considered, the OAA algorithm consists in the construction of K hyperplanes that separate respectively one class and the $K-1$ other classes. The OAO algorithm consists in the construction of $\frac{K(K-1)}{2}$ hyperplanes which separate each pair of classes. In the two cases the final label is the one which has been chosen the most often. The OAO algorithm has been retained for this application. They proposed extensions of binary SVM in order to directly manage the multiclass cases (Vapnik, 1998; Weston and Watkins, 1998; Bredensteiner and Bennett, 1999; Crammer and Singer, 2002; Hsu and Lin, 2002; Lee *et al.*, 2004; Guermur, 2007). These extensions represent an alternative to the methods implementing successive binary classifiers.

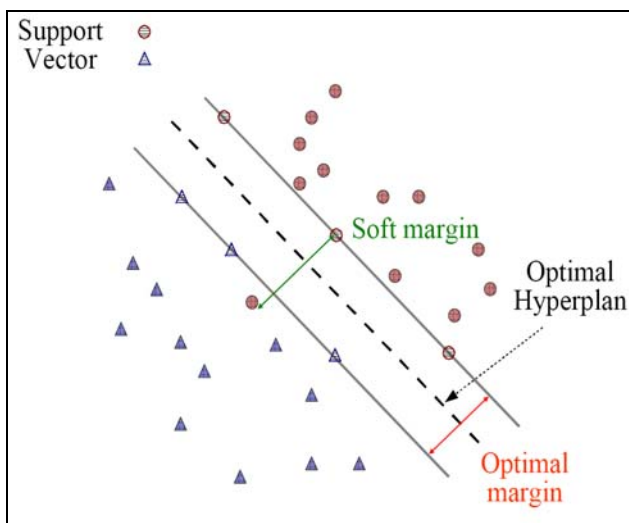


Figure 5. SVM classifier - linear case

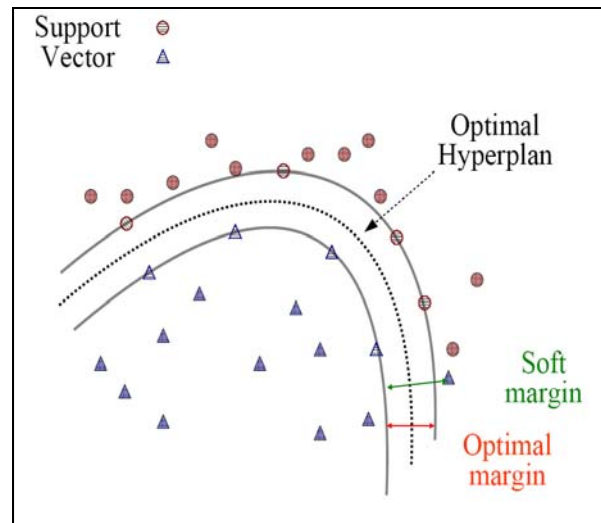


Figure 6. SVM classifier – non linear case

3.2. Hyperspectral

In this article, the hyperspectral is used to identify the main land cover classes of the floodable area in the situation of a low water level at the end of autumn/beginning of winter. Hyperspectral data is used to discriminate and map wetland vegetation at the species level (Belluco *et al.* 2006; Rosso *et al.*, 2005; Pengra *et al.* 2007; Vaiphasa *et al.* 2005 ; Adam *et al.*, 2009).

Hyperspectral processing and analysis techniques could be divided into two major approaches: "pixel by pixel" supervised classifications and object-oriented classifications. Nevertheless, processing hyperspectral images usually requires some special techniques for compressing and reducing spectral data. The CHRIS/PROBA image that we had at our disposal exhibited a lot of recording noise. This issue of analysis and reduction of the noise contained by the images has been permanently approached after the launching of CHRIS/PROBA satellite (Garcia and Moreno, 2004 ; Settle, 2001 ; Barducci and Pippi, 2001 ; Barnsley, Cutter, Lobb and Teston, 2005). Our CHRIS/PROBA image is affected by

two main noises (horizontal and vertical noises). According to a large number of studies, horizontal noise consists in the random loss of partial data from some lines oh the images and this noise is easy detect and correct using the horizontal profile of each file and the average of the nearest pixels to correct the bad values. Vertical noise or vertical striping is due to errors in the alignment of the sensors in the construction of the instrument. In the literature we can find a couple of methods to obtain the factors to correct this type of noise, and they are always based in the application of a filter in some point of the methodology, so that they have an important dependence with the image content (Garcia and Moreno, 2004). Thus, to the extent possible, it is desirable to improve the signal-to-noise (S/N) ratio by reducing or removing noise in the image data. In this study, noise was removed using the minimum noise fraction (MNF). The MNF transformation is a linear transformation related to PC that orders the data according to signal-to-noise-ratio (SNR). It determines the inherent dimensionality of the data, segregates noise in the data and reduces the computational requirements for subsequent processing. It partitions the data space into two parts: one associated with large eigenvalues and coherent eigenimages, and a second with near-unity eigenvalues and noise-dominated images. By using only the coherent portions in subsequent processing, the noise is separated from the data, thus improving spectral processing results (Kruse F. A., and *al.*, 1997).

For the traditional approach (pixel by pixel) a supervised classification was performed on the results of three processing techniques :

- a) Karhuen-Loeve transformation (PCA) applied on the 18 bands and subsequently recombination of four resulting axes.
- b) Minimum noise fraction (MNF) transformation applied on the 18 bands and subsequently recombination of four resulting axes.
- c) Statistical and visual analysis of the 18 bands and recombination of 12 of them.

The selection of the resulting axes, or transformed bands, after applying the PCA and MNF processing techniques, was based on their eigenvalues. For both methods, the first four axes were selected, however, the percentage of spectral information compressed in each axis is not similar as shown in table 3.

Table 3. Band wavelengths of the CHRIS instrument

Dataset		Danube water levels at Tulcea		Processing images	Objectives
Radar dataset ENVISAT/A SAR	19/04/2006 01/05/2006 08/05/2006	Floods (April/May)	4.29m 4.34m 4.15m	Georeferencing Filtering of speckle Define of the classes Classification SVM	Risk management Observation and mapping of flood hazard (<i>flooded areas</i>)
	13/06/2007	Drought (July)	1.47m	Data fusion	Forecast Observation and mapping of land cover floodable
Hyperspectral dataset PROBA/CH RIS	17/12/2004	Normal Conditions (December)	2.30m	Minimum noise fraction / PCA Segmentation Object-oriented Classification	Forecast Observation and mapping of land cover floodable

Table 4. Eigenvalues of the PCA and MNF selected

	PCA			MNF		
	<i>Eigenvalue</i>	%	$\Sigma\%$	<i>Eigenvalue</i>	%	$\Sigma\%$
Axe 1	561996241	77,81	98,15	57,949093	30,08	78,50
Axe 2	120285613	16,65		52,022116	27,01	
Axe 3	15641757,2	2,17		21,632524	11,23	
Axe 4	10946872,4	1,52		19,622974	10,19	

As to the last method for compressing hyperspectral data, the manual selection of the spectral bands was realized after individual analysis of each band and comparing the reflectance behaviour of preliminary land cover classes. Six bands were considered modestly useful for class distinction. Consequently, the selected bands are : 5, 6, 8, 10, 11, 12, 13, 14, 15, 16, 17 and 18.

Object-oriented processing techniques were initiated by a multisource data combination composed of: four PCA axes, four MNF axes and 12 selected bands. Afterwards, seven levels of segmentation were created and several classification tools (combining spectral and spatial criteria) were used for defining the land cover / land use classes.

Image segmentation is a main step in object-oriented classification because it creates the image objects. As proposed by the *Definiens* userguide, a well-suited approach when segmenting new data is to simply play with it, running different segmentations with different parameters until the result is satisfying. After several tests by visual analysis, the segmentation parameters were set using the weight of 0.9 for the color factor (consequently 0.1 for the shape factor) and 0.9 for the compactness factor (0.1 for the smoothness factor). The seven scale parameters performed were: 400 (biggest objects), 350, 300, 200, 100, 50 and 30 (smallest objects).

4. RESULTS AND DISCUSSION

4.1. Radar image analysis and processing

By using the radar data given by the recordings of the ENVISAT/ASAR sensor, the main objective of this section of this paper is to analyze the capacities offered by this sensor in terms of the spatial characterization of the flood hazard and flood mapping in terms of the signal polarization and radiometric and geometric resolution. This mapping gives useful information for the setting of parameters of the hydraulic models and may also represent an aid in the crisis management and flood forecast. Compared with certain entities (e.g.: SERTIT in Strasbourg, ZKI – Centre for Satellite Based Crisis Information of DLR, ROSA – Romanian Spatial Agency, etc.) that propose fast mapping services, our diachronic approach (before the peak of the flood - the peak - after the peak of the flood and after one year) belongs to a series of methodological papers bringing information equally about the period of water draining taking into account the general context of the event throughout the geographical, hydrographic, historical and land management parameters.

Starting from the idea that the response of radar for one flooded area may differ much from that of a moist soil, the implemented methodological chain primarily focuses on the potentialities of parallel polarization (VV) in terms of the reparability of different themes related to soil occupancy in moist areas and in flood condition. The signal polarized in VV may be retrodiffused by the flooded surfaces but, at the same time, it may be strongly disturbed by the rugosity induced by the wind and the partially submerge vegetation. In order to make our diachronic analysis, it was necessary to normalize the signal intensity. This normalization is ensured by the radiometric calibration of images. This process allows calculating, starting from the retrodiffused signal, a size without dimension called the retrodiffusion coefficient σ° . The retrodiffusion coefficient depends on the physical parameters of the surface and also on the sensor's parameters such as the incidence angle, polarization and the length of the radar wave. This retrodiffusion coefficient is generally expressed in decibel (dB). The average values observed in C band, VV polarization, usually range between -6dB and -8dB (Hawkins et al., 1999). In order to produce flood maps during the spring of 2006 in the Danube Delta, we carried out a radiometric analysis based on the ASAR data over the different flooded/non flooded areas with the help of different ground surveys. By remembering the format of our images - WSM (*Wide Swath Mode*) ascending and descending – the spatial resolution is 75mx75 m associated to a relatively good radiometric accuracy (corresponding to 21 « looks »). A temporal filtering followed by a spatial filtering allowed us to reduce the effects of «speckle» (noise

inherent to RADAR systems with opening synthesis). A nonlinear filter of Lee type was applied to the four ASAR images by maintaining the smallest possible filter size in order to limit as much as possible the degradation of the spatial resolution considering the objective of this activity - to isolate the flood fields. The georeferencing of the radar images starting from a LANDSAT TM5 optical image completed the pre-treatment stage.

The second treatment stage of the radar image proposes SVM supervised classifications starting from the radar images, on one hand, three ASAR images from 2006, and, on the other hand, three 2006 images with the only 2007 image.

The basic principle of this methodological part is to identify the temporal changes related to the state of the surfaces of the main classes of land cover under flood between 19/04/2006 and 08/05/2006. These temporal changes refer in fact to the changes of the retrodiffusion coefficient depending on the classes of land cover of the flooded soil and/or the moisture level of the soil. Because of the specular effect of the reflection of the radar wave on water, this type of surface appears very dark on the radar images. However, when the surface is not completely flat but it is disturbed by wind, it may appear in different grey hues thus rendering them more difficult to differentiate from other types of land cover. The main classes of land cover differentiated on the radar images of 2006 and 2007 were visualized in colorful composition of the radar images (on a given date, one image occupied a red, green or blue plane) which allowed us to determine 5 different classes for 2006 and 6 for 2007.

To create the different maps of the flood with the ASAR data, we applied the SVM classification on the intensities and their ratio. This SVM algorithm presented in the section related to methods of this article based on the theory of kernels allows for the solving of the linearly inseparable problems. It also allows us to take into account numerous and heterogeneous parameters.

Thus the flood map during spring 2006 (ASAR, 5 classes) is based on 6 primitives (parameters), the mapping of the period of 2006 and 2007 (ASAR, 6 classes) is based on 10 primitives. By remembering the role of the parameters used in this algorithm, they consider N the number of parameters characterizing a pixel. In case of a two class problem (every pixel of the image must belong either to class A or to class B), the objective of this problem is to find in the space of N size the optimal hyperplane separating the 2 classes (see the section *Methods* of this article). In our case, these parameters were established in relation with radiometry and the radiometric reports for diverse dates taken into consideration (for example for the classification combining 4 images, $N = 4$ radiometry + 6 radiometric reports = 10 parameters). The classes resulted from the first SVM classification (figure 7) notably refer to the flooded and drained areas up to the end of the floods: flooded areas, flooded and drained areas up to the end of the floods, wetland (1), wetland (2), permanent water. The second classification (figure 8) combining 3 images of 2006 floods and one image taken during the draught from 2007 shows one more class, the one regarding the bare soil or the lack of vegetation: flooded areas in 2006 and drained afterwards up to July 2007, flooded and drained areas up to the end of the floods, wetland (1), wetland (2), permanent water and bare soil and/or scarce vegetation.

Classification results present high-quality statistical values, as shown in table 5. Ground surveys confirm this accuracy. The choice of ground surveys has been made in relation with the onsite observations and informative inquiries run during the summer of 2007 for the population affected by these floods (figure 2) so as to reconstitute the size of the flooded fields. The map derived from all the ASAR data allows the estimation of the area that was drained between the end of spring 2006 and June 2007 (figure 8).

Interpretation of the radar results provides first the geographic location of the flooded areas (figures 7 and 2). Most localities covered by the floods of spring 2006 are in the sector of the fluvial delta (in its western part, figure 2), the oldest sector of the delta. The developments of the deltaic waters partially explain this spatial distribution. The localities mostly affected are on the branches that have never been diked. Generally, after every important flood, they built dikes, initiated either by the State (the local Council) or by the inhabitants or other dike owners. The pace distribution of the flooded areas also tells us about the dimension of the spring 2006 floods.

In certain localities (Tudor Vladimirescu, Gorgova, Partizani, figure 2) waters persisted 2 or 3 months (figure 2). The quantities of rain in June 2006 (72.3 mm) explain the difficult drainage of waters in these localities. In other regions (figures 7 and 8 the class in dark blue), the drainage took place much faster (between May 1st and May 8th 2006) due to the existence of a quite dense channel network, as well as around the locality Mila 23.

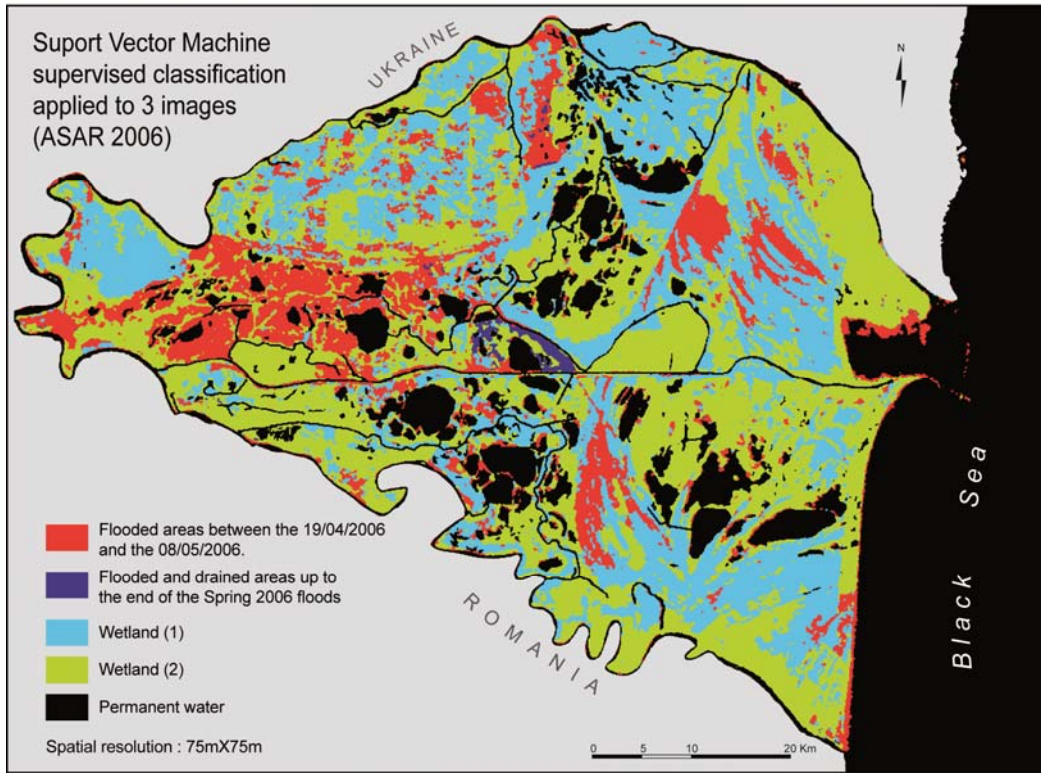


Figure 7. SVM Classification applied to 3 images (ASAR 2006)

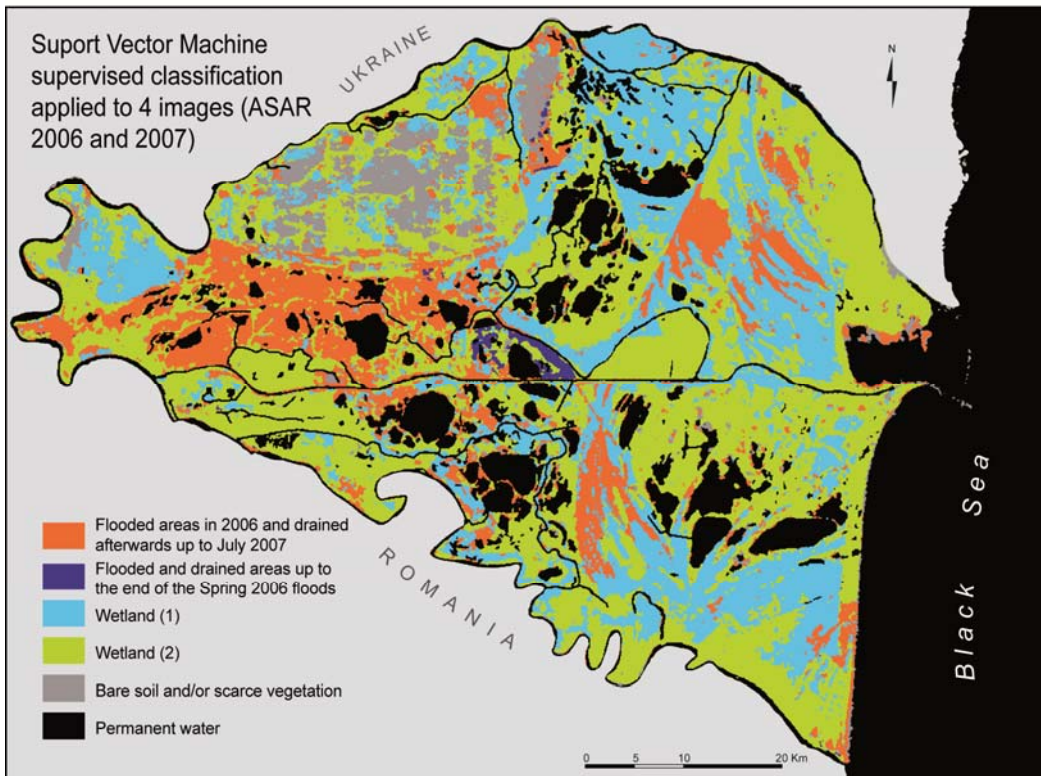


Figure 8. SVM Classification applied to 4 images (ASAR 2006 and 2007)

Table 5. Classification accuracy in %

	Spring 2006 (ASAR)	Spring 2006 (ASAR) and July 2007 (ASAR)
Flooded areas between the 19/04/2006 and the 08/05/2006	100	100
Flooded and drained areas up to the end of the Spring 2006 floods	98	97
Wetland (1)	97	92
Wetland (2)	96	92
Permanent water	99	99
Flooded areas in 2006 and drained afterwards up to July 2007	x	86
Mpa	98	95

4.2. Hyperspectral image analysis and processing

If the radar approach gives us precise information on the location of the flooded areas, in exchange this instrument immediately shows its limits when it comes about the areas liable to flooding and the classes of land cover, areas of outstanding importance for any land management project. A second complementary hyperspectral approach contributing to the characterization of the floodable areas is presented through the images resulted from the records of PROBA satellite with its compact instrument, Chris, capable of offering details about the vegetal surfaces of this moist area (its resolution reaches 18 m by associating up to 19 spectral bands). A correlation table between the classes detected through the radar and hyperspectral data has been implemented so as to facilitate the comprehension of the methodological chain (table 6).

As mentioned in the dataset presentation, hyperspectral analyses were concentrated in the central part of Danube Delta. This area, situated in the north side of the Sulina branch and neighboring the Mila 23 settlement, was particularly affected by the 2006 floods (figure 2 and 7). The hyperspectral map classes associate both land cover and land use aspects, a special effort was dedicated for detailing deltaic vegetation. The different types of reed classes are mostly characterized by human activities like burning and cutting reed vegetation, and the periods of these interventions are also important for comprehending the dynamics of this geographic space.

Different segmentation levels were useful for classifying image objects. The final object-oriented classification was performed on the second segmentation level (scale factor = 50) ; however, several class hierarchical conditions set for this level depend on higher segmentation level objects (figure 9). The *Definiens* program also offers the possibility of combining spectral and spatial parameters (individually for each class) in the classification process.

A first general classification was performed on level 7 (biggest objects). The main goal was to separate the image into three major classes: I- Deltaic vegetation, II-Settlement or managed zones and III-Water. All the other classes created in the lower levels (more detailed) were associated to one major class. This notion of hierarchical groups can be visualized in the legend of figure 10. The final object-oriented classification includes eleven classes, which are organized into a logical and interrelated scheme.

This kind of map provides detailed information about flooded and floodable zones; land cover and land use aspects are associated. The multilevel segmentation allows us to adapt the level of detail of the map according to specific requests. This part of the Danube Delta presents important social dynamics and human activities transform the landscape quickly. In this case, qualitative and comparative analyses were privileged for assessing the positive and negative aspects of the different hyperspectral processing and analyzing techniques applied in the present research.

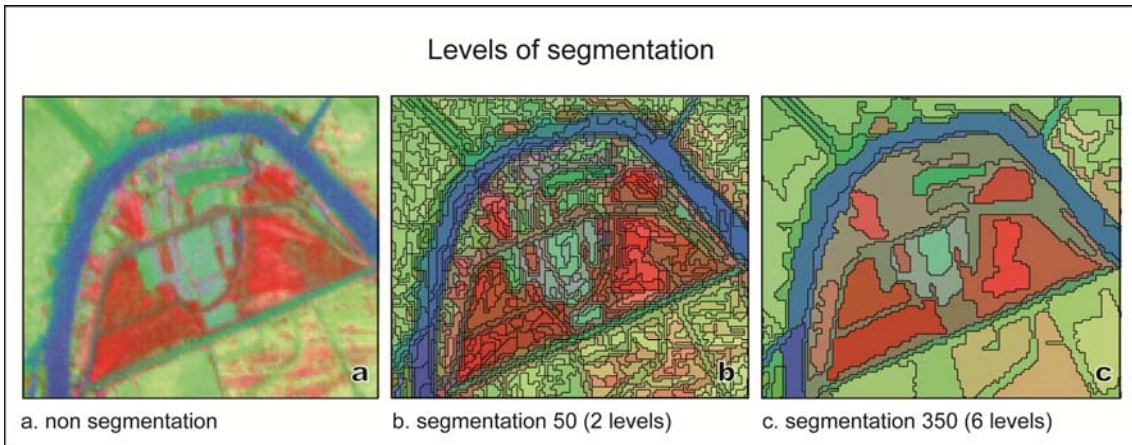


Figure 9. Levels of segmentation: a). non segmentation; b). segmentation 50 (2 levels); c) segmentation 350 (6 levels).

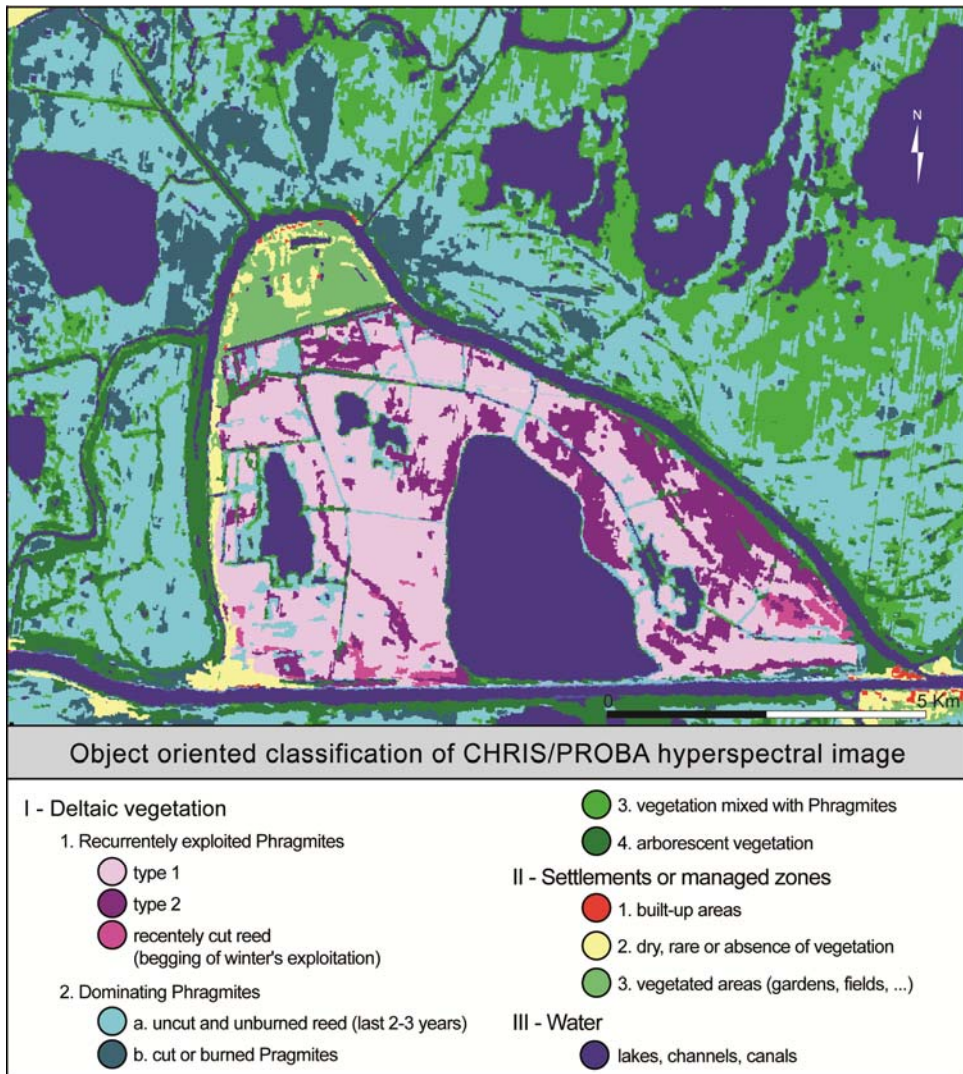


Figure 10. Object-oriented classification

Table 6. Description Radar Classification and Hyperspectral Classification

Radar Classification	Hyperspectral Classification	
Flooded areas between the 19/04/2006 and the 08/05/2006	Flooded area (in 2006) and Floodable areas	Recurrantly exploited Phragmites
Flooded and drained areas up to the end of the floods		Recurrantly exploited Phragmites
Wetland (1)	Floodable areas	Dominating Phragmites Cut or burned Phragmites Settlements or managed zones
Wetland (2)	Areas unaffected by the floods 2006	Vegetation mixed with Phragmites Arborescent vegetation

5. CONCLUSIONS AND PERSPECTIVES

With its different modes of functioning and acquisition, the ENVISAT satellite radar confirms the capabilities of the radar sensor for describing and mapping flood areas. The VV polarization used in our application appears as a strong contributor in the delimitation of flood extent, but it requires manual interpretation and good field knowledge. The use of other polarizations such as those offered by ASAR HH or HV would certainly improve the discrimination of the different areas affected by floods. The HH polarization especially allows better discrimination between water surfaces and terrestrial surfaces as studies involving RADARSAT-1 images have shown. An interesting perspective is also given by RADARSAT-2, due to its right and left viewing modes; this satellite increases the availability of optimal data for the mapping of floods. Moreover, its full polarimetric capacities might contribute to the enhancing of the quality of information related to the floods of lands and woodlands. In the section Risk management, methodological aspects regarding the tridimensional characterization of the flood hazard and, with the help of hydrologic modeling, the combination RADARSAT-2/LIDAR might represent an element of novelty. Knowing the water levels by modeling and using the numerical land model offered by LIDAR measurements, the determination of the flooded areas and their submersion level may be possible. On the other hand, the new PALSAR fully polarimetric radar sensor aboard the ALOS satellite (L band, launched in January 2006) offers very interesting perspectives in terms of land cover liable to flooding, thus in terms of risk forecast. The fully polarimetric sensors allow the simulation of an acquisition made by a sensor whatever the polarization configuration: linear polarization HH, HV, VV, as in the case of ASAR, but also parallel or crossed circular polarizations. The degrees of polarimetric coherence showed, for instance, great potential in the discrimination of the diverse soil types. Moreover, the highest acquisition wavelength ($\lambda = 24 \text{ cm}$) of this sensor offers complementarity with ASAR ($\lambda = 5.6 \text{ cm}$), which is very interesting for mapping flooded areas.

Information obtained on the distribution of flood areas should be useful for crisis managers and it is also useful after the event in the evaluation of the impacts from a financial, material and human standpoint. This damage evaluation stage needs to describe the landscapes and to have information on the affected populations.

Hyperspectral images, such as CHRIS/PROBA, certainly present numerous applications in different science domains, but for the characterization of the areas liable to flooding, it turns out to be an instrument adapted and capable to give important details on the land cover of the vegetal soil which is in certain areas the main class liable to flooding. Hyperspectral data is potentially rich but for reaching satisfactory results, the processing techniques should be adapted. The object-oriented approach shows encouraging results but pixel by pixel image processing also offers some interesting tools. As to CHRIS/PROBA data, exploring the multiple angle images should improve classification quality. Using multitemporal images (ideally one for each season) is also suggested for overall comprehension of vegetation behavior and human related activities.

With the numerous recent and upcoming SAR satellite missions and promising multisensor constellations (SWOT, TerraSAR-X, COSMOSkyMed, and Sentinel-1), timelier image delivery will be possible, and a new era of SAR-derived flood services can be envisaged.

6. REFERENCES

- Adam, E., Mutanga, O., Rugege, D., Multispectral and hyperspectral remote sensing for identification and mapping of wetland vegetation: a review, In *Wetlands Ecology Management*, Springer, 2009, 281-296p.
- Alsdorf, D., Rodriguez, E. and Lettenmaier, D. (2007), Measuring surface water from space, *Reviews of Geophysics*, v45, n2, pp. RG2002.
- Aronica, G., Hankin, B. and Beven, K., Uncertainty and equifinality in calibrating distributed roughness coefficients in a flood propagation model with limited data, *Adv. Water Resour.*, vol. 22, no. 4, pp. 349–365, Dec. 1998.
- Baatz, M. et Schäpe, A. (2000), Multiresolution Segmentation – an optimization approach for high quality multi-scale image segmentation. In Strobl, B. et al., G.A. G. I., editors, *Beiträge zum AGIT-Symposium Salzburg 2000*, Karlsruhe, Herbert Wichmann Verlag, pages 12–23,
- Baatz, M., Benz, U., Deghani, S., Haynena, M., Höltje, A., Hofmann, P., Lingenfelder, I., Mimler, M., Sohlbach, M., Weber, M. and Willhauck, G. (2004). *eCognition User Guide 4*. Definiens Imaging GmbH, Munich, 110p.
- Barducci, A., and Pippi, I. Analysis and rejection of systematic disturbances in hyperspectral remotely sensed images of the Earth. *Applied Optics*, Vol. 40, pp. 1464 – 1477, 2001.
- Barnsley, M.J., Settle, J.J., Cutter, M. Lobb, D. and Teston, F. (2005), The PROBA/CHRIS mission: a low-cost smallsat for hyperspectral, multi-angle, observations of the Earth surface and atmosphere, *IEEE Transactions on Geoscience and Remote Sensing*, 40(7): 1560-1573.
- Bannari, A., Pacheco, A., Staenz, K., McNairn, H. and Omari, K. (2006) Estimating and Mapping Crop Residue Cover in Agricultural Lands Using Hyperspectral and IKONOS data. *Remote Sensing of Environment*, vol. 104, p. 447-459.
- Bonn, F., and R. Dixon (2005), Monitoring flood extent and forecasting excess runoff risk with RADARSAT-1 data, *Nat. Hazards*, 35, 377–393.
- Belluco, E, Camuffo, M, Ferrari, S, Modenese, L, Silvestri, S, Marani, A, Marani, M (2006) Mapping salt-marsh vegetation by multispectral and Hyperspectral remote sensing, *Remote Sens Environ* 105:54–67.
- Bishop, C. (2006). *Pattern Recognition and Machine Learning*. Berlin: Springer.
- Brakenridge, G. R., Tracy, B. T. and J. C. Knox (1998), Orbital SAR remote sensing of a river flood wave, *Int. J. Remote Sens.*, 19(7), 1439–1445.
- Bredensteiner, E. et Bennett, K. (1999), Multicategory Classification by Support Vector Machines, *Computational Optimizations and Applications*, 12(1-3), pp. 53–79.
- Brivio, P.A., Colombo, R., Maggi, M. and Tomasoni, R. (2002), Integration of remote sensing data and GIS for accurate mapping of flooded areas, *Int. J. Remote Sens.*, vol. 23, no. 3, pp. 429–441.
- Brown, R.J., Wood, D., Brisco, B. (1997), Mapping rainfall distribution using RADARSAT data, *Proceedings of GER'97, Geomatics in the ERA of RADARSAT*, Ottawa, 9p.
- Burges, C-J. (1998). A tutorial on support vector machines for pattern recognition, in *data mining and knowledge discovery*. U. Fayyad, Ed. Kluwer Academic, 1-43.
- Cortes, C. and Vapnik, V. (1995), *Support vector networks. Machine Learning*, 20: 273–297.
- Crammer, K. et Singer, Y. (2002), On the algorithmic implementation of multiclass kernel-based vector machine, *Journal of Machine Learning Research*, 2, pp. 265–292.
- Cutter, M.A. (2004). A low cost hyperspectral mission. *Acta Astronautica*. 55, 631-636.
- Adam, E., Mutanga, O., Rugege D. (2009), Multispectral and hyperspectral remote sensing for identification and mapping of wetland vegetation, *Wetlands Ecology and Management*, Volume 18, Number 3, p281-295.
- Fellah, K., Mesures de paramètres des sols à partir de données des satellites radar pour les applications hydrologiques, Thèse de doctorat, Univ. Louis Pasteur, 1997, 213p.
- Fukuda, S. and Hirose, H. (2001), Support vector machine classification of land cover: application topolarimetric SAR data. *Geoscience and Remote Sensing Symposium*. 1, 187-189.
- Garcia, J.C., Moreno, J. (2004), Removal of noises in CHRIS/PROBA images: application of the Sparc Campaign data, *Proc. of the 2nd CHRIS/Proba Workshop, ESA/ESRIN, Frascati, Italy*, 5p.
- Gruntfest, E., Handmer, J. (dir.) (2001), *Coping with flash floods*, NATO science series, Kluwer Academic Publisher, 322p.
- Guermeur, Y. (2007), *SVM Multiclasses, Théorie et Applications*. Habilitation à Diriger des Recherches, HAL – CCSD, 91p.
- Hawkins, R K, Attema, E, Crapolicchio, R, Laur, H, Lecomte, P, Meadows, P J, Srivastava, S K (1999), Stability of Amazon Backscatter at C-Band: Spaceborne SAR Results from ERS-2 and Radarsat-1, CEOS SAR, Workshop 2-29 October 1999, ESA-SP450.
- Horritt, M. S. (2000), Calibration of a two-dimensional finite element flood flow model using satellite radar imagery, *Water Resour. Res.*, vol. 36, no. 11.
- Hostache, R., Puech, C., and Raclot, D. (2005), Caractérisation spatiale d'aléa inondation à partir d'images satellites radar: Cartographie et estimation de niveaux d'eau par fusion des données images avec des données topographiques, paper presented at International Conference on Spatial Analysis and Geomatics, UMR ESPACE, Avignon, France, 12p.
- Hostache, R., Matgen, P., Schumann, G., Puech, C., Hoffmann, L., and Pfister, L. (2009), Water level estimation and reduction of hydraulic model calibration uncertainties using satellite SAR images of floods, *IEEE Trans. Geosci. Remote Sens.*, 47, 431–441.
- Hsu, C.-W. et Lin, C.-J. (2002), A comparison of methods for multi-class support vector machines. *IEEE Transactions on Neural Networks*, 13(2), pp. 415–425.

- Jung, A., Kardevan, P. and Tokci, L. (2004). Detection of urban effect on vegetation in a less built up Hungarian city by hyperspectral remote sensing. *Physics and Chemistry of the Earth*. 30, 255-259.
- Kanevski, M., Pozdnoukhov, A. and Timonin, V., 2009, *Machine Learning for Spatial Environmental Data : theory, applications and software*, EPFL Press, 2009, 377 p.
- Koutroumbas, K. and Theodoridis, S. (2008). *Pattern Recognition* (4th ed.). Boston: Academic Press, 340p.
- Kruse, F. A., Richardson, L. L., and Ambrosia, V. G., Techniques Developed for Geologic Analysis of Hyperspectral Data Applied to Near-Shore Hyperspectral Ocean Data. Presented at the Fourth International Conference on Remote Sensing for Marine and Coastal Environments, Orlando, Florida, 17 – 19 March, 1997, 14p.
- Laugier, O., Fellah, K., Tholey, N., Meyer, C. and De Fraipont, P. (1997), High temporal detection and monitoring of flood zone dynamic using ERS data around catastrophic natural events: The 1993 and 1994 Camargue flood events, paper presented at 3rd ERS Symposium on Space at the Service of Our Environment, Eur. Space Agency, Florence, Italy, <http://earth.esa.int/workshops/ers97/papers/laugier/>.
- Lee, J. S., Grunes, M. R and de Grandi, G. (1999). Polarimetric SAR speckle filtering and its implication for classification IEEE Trans. *Geosci. and Rem. Sens.* 37(05), 2362-2373.
- Lee, Y., Lin, Y. and Wahba, G. (2004), Multicategory Support Vector Machines : Theory and Application to the Classification of Microarray Data and Satellite Radiance Data. *Journal of the American Statistical Association*, 99(465), pp. 67–81.
- Marinelli, L., Michel, R., Beaudoin, A. (1997), Flood mapping using ERS tandem coherence image : a case study in souther France. In *third ERS Symposium on Space at the service of our environment*, Florence, Italie, 17-21 march 1997, p. 531-536.
- Matgen, P., Henry, J.-B., Pappenberger, F., de Fraipont, P., Hoffmann, L., and Pfister, L. (2004), Uncertainty in calibrating flood propagation models with flood boundaries derived from synthetic aperture radar imagery, in Proc. 20th Congr. Int. Soc. Photogramm. Remote Sens., Istanbul, Turkey, 352–358.
- Matgen, P., Schumann, G., Henry, J.B., Hoffmann, L. and Pfister, L. (2007). Integration of SAR-Derived Inundation Areas, High Precision Topographic Data and a River Flow Model Toward Real-Time Flood Management, *Journal of Applied Earth Observation and Geoinformation*, 9, 247–263.
- Nico, G., Pappalepore, M., Pasquariello, G., Refice, A., Samarelli, S. (2000). Comparison of SAR amplitude vs. coherence flood detection methods a GIS application. *International Journal of Remote Sensing* 21(8): 1619-1631.
- Oberstadler, R., Hönsch, H., Huth, D. (1997), Assessment of the mapping capabilities of ERS-1 SAR data for flood mapping: a case study in Germany, Hydrological Processes, vol.11(10), 1415-1425.**
- Pappenberger, F., Beven, K., Horritt, M. and Blazkova, S. (2005), “Uncertainty in the calibration of effective roughness parameters in HEC-RAS using inundation and downstream level observations,” *J. Hydrol.*, vol. 302, no. 1–4, pp. 46–69, Feb. 2005.
- Pasterik, E.T. (2000), The national flood insurance program: a U.S. approach ti flood loss reduction in Marsalek et al. (dir.), in *Flood issues in contemporary water management*. NATO Science series, 2, Environmental security, vol. 71, Kluwer Academic Publishers, 185-195.
- Pengra, BW, Johnston, CA, Loveland, TR (2007) Mapping an invasive plant, *Phragmites australis*, in coastal wetlands using the EO-1 Hyperion hyperspectral sensor. *Remote Sens Environ* 108:74–81.
- Puech, C. and Raclot, D. (2002), Using geographical information systems and aerial photographs to determine water level during floods. *Hydrological Processes*, Vol. 16 (08), 1593-1602.
- Rosso, PH, Ustin, SL, Hastings, A (2005) Mapping marshland vegetation of San Francisco Bay, California, using hyperspectral data. *Int Journal Remote Sens* 26:5169–5191.
- Schmidt, KS, Skidmore, AK (2003) Spectral discrimination of vegetation types in a coastal wetland. *Remote Sensing Environ* 85:92–108.
- Schumann, G., Henry, J. B., Hoffmann, L., Pfister, L., Pappenberger, F., and Matgen, P. (2005), Demonstrating the high potential of remote sensing in hydraulic modelling and flood risk management, Annual Conference of the Remote Sensing and Photogrammetry Society With the NERC Earth Observation Conference, Remote Sens. and Photogramm. Soc., Portsmouth, U. K.
- Schumann, G., Di Baldassarre, G., Bates, P.D. (2009), The Utility of Spaceborne Radar to Render Flood Inundation Maps Based on Multialgorithm Ensembles, in *IEEE Trans. Geoscience and Remote Sensing*, vol. 47, n°8, pp.2801-2807.
- Shawe-Taylor, J. and Cristianini (2004), N. Kernel Methods for Pattern Analysis. Cambridge University Press, 460p.
- Schohn, G. et Cohn, D. (2000), Less is more : Active learning with support vector machines. In *Proceedings of the Seventeenth International Conference on Machine Learning*, p. 839–846.
- Smola, A.J. and Schölkopf, B. (1998), A tutorial on Support Vector Regression, *NeuroCOLT2 Technical Report Series*, NC2-TR-1998-030. October 1998, 71p.
- Ulaby, F. T., Brisco, B., Dobson, C. (1983). Improved spatial mapping of rainfall events with spaceborne SAR imagery, *IEEE Transactions on Geoscience and Remote Sensing*, Vol. GE-21(1), pp. 118-121.
- Ulaby, F. T. and Elachi, C. (1990). *Radar polarimetry for geoscience applications*. Artech House ed., 364p., <http://www.csie.ntu.edu.tw/~cjlin/libsvm>.
- Vaiphasa, CK, Skidmore, KA, de Boer, WF, Vaiphasa, T (2007), A hyperspectral band selector for plant species discrimination. *ISPRS J Photogramm Remote Sensing* 62:225–235.
- Vapnik, V. (1995), *The Nature of Statistical Learning Theory*, Springer-Verlag, New York, Inc., New York, USA.
- Vapnik, N. (1998). *Statistical Learning Theory*. Springer-Verlag, New York, Inc., New York, USA.

- Vidal, J.-P., 2005, Validation opérationnelle en hydraulique fluviale - Approche par un système à base de connaissance, Thèse de doctorat, Institut National Polytechnique de Toulouse, HHLY-Cemagref, 303 p.
- Weston, J. and Watkins, C. (1998), Multi-class Support Vector Machines, Technical report, Royal Holloway, University of London, Egham, UK.
- Yésou, H., Chastanet, P., Fella, K., Jranblanc, Y., De Frainpont, P. & Bequinon, J. (2000), Contribution of ERS SAR images and ERS coherence data to a flood information system on the Meuse basin – France, in European Space Agency, (Special Publication) ESA SP, 597-605.